



HAL
open science

Elaboration of Activated Carbon/Titanium dioxide granular composites by mechanosynthesis: effect of the composition on the sorption capacity and photocatalytic efficiency

Enrique Ribeiro, Gaël Plantard, V. Goetz

► **To cite this version:**

Enrique Ribeiro, Gaël Plantard, V. Goetz. Elaboration of Activated Carbon/Titanium dioxide granular composites by mechanosynthesis: effect of the composition on the sorption capacity and photocatalytic efficiency. *Journal of Photochemistry and Photobiology A: Chemistry*, 2021, 408, pp.113108. hal-03369283

HAL Id: hal-03369283

<https://cnrs.hal.science/hal-03369283v1>

Submitted on 7 Oct 2021

HAL is a multi-disciplinary open access archive for the deposit and dissemination of scientific research documents, whether they are published or not. The documents may come from teaching and research institutions in France or abroad, or from public or private research centers.

L'archive ouverte pluridisciplinaire **HAL**, est destinée au dépôt et à la diffusion de documents scientifiques de niveau recherche, publiés ou non, émanant des établissements d'enseignement et de recherche français ou étrangers, des laboratoires publics ou privés.

Elaboration of Activated Carbon/Titanium dioxide granular composites by mechanosynthesis: effect of the composition on the sorption capacity and photocatalytic efficiency

E. Ribeiro^(*,1,2), G. Plantard^(1,2), and V. Goetz⁽¹⁾

⁽¹⁾ PROMES CNRS, UPR 8521, Rambla de la thermodynamique 66100 Perpignan, France.

⁽²⁾ University of Perpignan Via Domitia, 52 Paul Alduy 66100 Perpignan, France.

* Corresponding author. Tel.: +33602311658;

E-mail address: enrique.ribeiro@promes.cnrs.fr

Abstract

Activated-Carbon/Titania composites (AC/TiO₂) is a relevant option to gather the dual adsorption/photodegradation property within a single material. This work aimed to investigate the composition influence on the adsorption and photodegradation properties of AC/TiO₂ composites against caffeine. TiO₂ grafted AC powders covering the whole composition scale were synthesized by a one-step mechanical milling process. This original simple elaboration route led to the obtention of powders which particles size and composition were homogeneous and well controlled. When the adsorbent mass ratio varied in the range 0.01- 0.75, the adsorption properties, i.e. apparent kinetic and maximum adsorption capacity of the composites increased respectively by 1 and 2-log. At the opposite, the photo-oxidation rate decreased significantly when the adsorbent ratio increased. The simple elaboration route explored produces flexible AC/TiO₂ composites with adjustable properties that can easily be managed to meet the requirements of different target applications.

1. Introduction

The common denominator for applications based on a solar photoreactor is solar resource management [1,2]. Whether photo processes are used for heat production (concentrated solar plants, domestic hot water), electricity production (solar power plants, photovoltaic panels) [3-5] or water photo-oxidation (photocatalysis, photo-fenton treatment) [6,7], their capacities are directly dependent on sunlight conditions. Discontinuities in the solar resource are classified according to several scales, i.e. day/night cycles, seasonal cycles, and annual cycles, but also meteorological conditions, and chiefly cloudiness, which have a strong impact on the characteristics of the solar resource (flux density, spectral distribution, diffuse and direct radiation) exploitable by the various processes [2]. For energy production, scientists working in collaboration with industry have developed solutions that consist in storing energy in the form of either electricity (batteries) or heat (sensible or latent heat) [3,8,9]. In photo-oxidation wastewater treatment processes, these technologies produce radicals, which are extremely reactive species capable of mineralizing all carbon compounds in a non-selective manner. Heterogeneous photo-oxidation, which is part of the family of advanced oxidation processes along with photo-fenton and ozonation processes, generates radicals from a photocatalyst [10-12], which for most industrial and academic applications is TiO_2 [7,13]. The principle consists in photo-exciting the semiconductor: the absorption of photons releases an electron-hole pair that reacts with the surrounding molecules to form radicals. This mechanism is effective but very short-lived, as radicals have only nanosecond lifetimes [10,11]. Unlike chlorine, which has a residual effect that delays treatment, the radicals get consumed instantly, which is a major bottleneck to using the solar resource where discontinuities operate on a scale of an hour (cloudy passages) to a day (day/night cycle). To overcome this constraint tied to the discontinuities of solar radiation, the solution lies in storing pollutants during night or low-sunlight phases in order to oxidize both stored pollutants and those continuously arriving from the flow of water during high-sunlight phases [14-17].

Technological solutions proposed at the process scale consist in designing hybrid processes that combine a storage process (e.g. column adsorption, membrane separation) with a photo-oxidation treatment process (photo-fenton, UV-ozonation, photocatalytic oxidation) [18-21]. This option consists of operating in two steps, where step one is a separation of the water matrix and contaminants, and step two is an oxidation of these contaminants (concentrated in an effluent or adsorbed on a sorbent). This kind of scheme has, for example, given rise to

experimentations consisting of a separation phase on an activated carbon (AC) column and then photo-oxidation-driven regeneration of adsorbents [22-25] or the treatment of an effluent previously separated and concentrated by a membrane process [21]. Such a concept is hugely advantageous, as it makes it possible to smooth the effects of resource intermittencies by dissociating the separation and treatment steps in time and space [15,19]. The main bottleneck to this approach is the inertia generated by the addition of storage, destocking and oxidation of water or contaminant-loaded adsorbent phases. This limitation is further compounded by slow sorption and photo-oxidation kinetics.

To break this deadlock, the avenues of research envisaged by the scientific community are moving towards the development of small-scale composites. The aim is to design hybrid materials made up of the two components, namely an adsorbent capable of storing molecules and a photocatalyst to drive the production of radicals. At particle scale, these materials have the dual sorptive and oxidative functionality. Such an association makes it possible to manage molecules *in situ* by playing on the reversibility of the balance between liquid and adsorbed phases [15,26]. The applications targeted are regeneration of these composites by photo-oxidation of the molecules stored on the adsorbent or use of these composites in molecule sorption cycles during the low-irradiation phases (clouds, night) and oxidation during the high-irradiation phases. Finally, it can also be assumed that the role played by the adsorbent in the photo-oxidation mechanism can have a synergistic effect. Several studies have set out to find a synergy that improves catalyst performance [10,11,29]. Even if the coupling of adsorbent materials with a catalyst is not yet well defined, studies are unravelling the mechanisms involved [30], and they show that this synergy can manifest in different ways. First, the presence of an adsorbent near the catalyst generates a high concentration gradient during the sorption phase that can greatly accelerate the transfer of molecules to the catalyst surface [31-33]. Another possibility is that the presence of adsorbed molecules substantially increases the local concentration of molecules in the vicinity of the catalysts. In this sense, studies tend to show that if the composition and size criteria of the two entities are respected, it is possible to improve mineralization rates by increasing the concentration of pollutant in the vicinity of the photocatalyst.

The next challenge is to choose a high-performance adsorbent, i.e. with high sorption and rate capacities. Studies have investigated a wide range of different adsorbents, but the most suitable candidate is activated carbon [34]. Activated carbon displays a porosity that develops a huge specific surface area (500 to 2000 m².g⁻¹), giving it a strong adsorbent capacity. It has

a microporous network, which is the site of the sorption reaction [35], and a mesoporous network, which makes the pollutant accessible to the adsorption site [30, 36]. Research has worked to improve these structural properties (porosity, specific surface area, microporosity) [37], which make it the most widely used adsorbent material in applied science and industry and the most suitable candidate for solar water treatment application [38].

To fully address this theme, describe and understand the mechanisms involved, the research has mainly focused on the association of activated carbon with titanium dioxide, which requires the development of efficient methods of preparing AC/TiO₂ composites that maintain the adsorbent capacity of the activated carbon and the photo-activity of the TiO₂ catalyst. There has been much research into methods for associating these two entities, with various applications [12, 39]. The main techniques are plasma deposition processes (CVD, PACVD) and soft methods (sol-gel, hydrothermal, impregnation) [29, 40, 41]. These techniques are functionalization methods, producing thin or nanostructured films that confer the adsorbents with new properties. The results obtained in terms of oxidation and storage capacity are satisfactory. They show that degradation capacities are improved [27,32, 42] and that activated carbon coated with a catalyst can undergo several storage/regeneration cycles [15]. Very recently, work has shown the possibility of combining activated carbon and a photocatalyst by mechanical synthesis [43]. This original path, based on the mechanical and ballistic action of mill balls, generates the formation of particles in the form of aggregates. Preparing granular composites requires firm control of the operating conditions (time, nature of the balls, composition of the mixture) [44]. Mechano-synthesis offers the possibility of developing compositionally-varied AC-TiO₂ composites using the same single method while preserving the original properties of each component. Unlike the methods traditionally considered (CVD, sol-gel) for functionalizing activated carbon surfaces, mechano-synthesis leads to composites that combine both components in the same volume. It is therefore possible to control the properties of the composite by scanning compositions from 0 (catalyst alone) to 1 (carbon alone) using a single method and set of operating conditions.

To meet the constraints of using the solar resource, the aim is to be able to manage the impact of discontinuities in sunlight by smoothing out variations in concentrations of molecules in the liquid. Here we set out to control the functional properties of composites, such as sorption capacity, transfer rate and oxidation capacity. Modifying the composition of the composites—and, critically, the adsorbent/catalyst ratio—makes it possible to direct their functional properties to the target applications, which here is large storage, regeneration and/or photo-

oxidation capacity. This work will be based on mechanosynthesis, which is a totally original method for the preparation of composites combining adsorbents with photocatalytic nanoparticles. This method make it possible to prepare composites that cover the entire range of compositions (from activated carbon alone to catalyst alone) and to compare their ability to adsorb and/or photo-oxidize between themselves but also against references materials, i.e. pure AC and pure TiO₂. We thus propose an experimental study to emerge the role of the adsorbent/catalyst pair and the role of composition as a shaper of functional properties. As we aim to demonstrate the value of varying the composition, our experimental measurements of sorption and oxidation capacity and their associated rates (transfer and oxidation rate) will be treated with simple models from the literature. The results can thus be compared to identify the effects related to the mechanosynthesis-process operating conditions and the effects related to composition. Prior to this comparative study, the AC/TiO₂ composites will be studied in terms of compositional properties, grain size and size distribution with the objective of developing repeatable composites that preserve the characteristics of the two original components.

2. Composites preparation

AC/TiO₂ composites were synthesized from commercial AC and TiO₂ powders. Picahydro SP23 (Pica, France) AC was selected for its capacity to remove micropollutants like volatile organic compounds or industry solvents from water by adsorption. This AC resulting from physical activation of coconut shell is characterized as having a high specific area of around 1000 m²/g and a millimetric-scale mean particle size. Aeroperl® P25 was chosen as the TiO₂ material for its high photodegradation capacity due to the controlled crystalline phase composition, which is described by the supplier as composed of 80wt% anatase and 20wt% rutile. The Aeroperl® P25 product also presents controlled powder granulometry (25 μm average diameter aggregates constituted of nanometric crystallites [45]).

2.1. Synthesis process

AC/TiO₂ composites were prepared by mechanosynthesis with a Fritsch Pulverisette 6 planetary ball mill. The highly-refractory and hard ceramic zirconia was selected as material for grinding-bowl and milling-ball components. Synthesis was performed in a 45 mL grinding bowl using small 3 mm-diameter milling balls. The ball-to-powder mass ratio chosen was the most common ratio for this type of preparation [46]. The rotary speed of the planetary ball mill was set at a fixed 400 rpm to stay below the upper speed limit at which the balls no longer

collide inside the mill but roll on the inner wall [44]. The milling protocol was composed of 5 min break after every 15 min of milling, for a total milling time of 10h. The whole set of parameters was chosen from optimization work that afforded a homogeneous AC/TiO₂ composite powder with repeatable granulometry without losing the adsorption and photodegradation properties of the starting materials [43]. A set of five initial AC/TiO₂ powder mass ratios was selected to cover a broad scale of compositions. Furthermore, two unmixed samples were prepared in the same way but with pure TiO₂ and pure AC as starting powder materials instead of a mix of both. These mechanosynthesized materials were named M_TiO₂ for ‘Milled TiO₂’ and M_AC for ‘Milled AC’, and served to limit the composition domain for the study on the properties of the composite materials. AC weight percentages in the as-made composites were as follows: 1, 5, 15, 30 and 75wt% of AC (the rest of the composite mass being TiO₂). For the purposes of this work, the composites were named 1_AC/TiO₂, 5_AC/TiO₂, 15_AC/TiO₂, 30_AC/TiO₂, and 75_AC/TiO₂, thus discriminating each composite based on the percentage weight of AC as given by the number prefixing the name. For each sample, the powder mixture was put in the zirconia mill and the process ran under ambient atmospheric pressure and temperature conditions.

2.2. Characterizations

Size and shape of the synthesized AC/TiO₂ composites were analyzed by Scanning Electron Microscopy (SEM-FEG, Hitachi S-4500). Images were acquired with a secondary electron detector and a 5 kV electron beam, at a working distance of 5 mm. A $\times 50\,000$ magnification was used to compare the shapes of different sample particles. The $\times 50,000$ magnification images (Fig. 1) highlight very clear differences in morphology from one AC/TiO₂ composition to another. The 1_AC/TiO₂ sample was composed of big aggregate-shaped particles (micron-scale) covered by nanometric components which were mostly TiO₂ particles. AC was indistinguishable on the particle surface, suggesting that the carbon component is located inside these aggregates. The 15_AC/TiO₂ sample image showed that increasing carbon content from 1wt% to 15wt% did not change the final particle shape but did lead to distinguishably faceted-shape AC particles at the surface of 15_AC/TiO₂ aggregates. The 30_AC/TiO₂ sample, and the 75_AC/TiO₂ sample in which TiO₂ was not the dominant surface compound, had different-shaped aggregates composed of one or more big micron-sized AC particles heterogeneously covered by TiO₂. They also displayed different AC coverage ratios: coverage decreased with increasing carbon content. Ultimately, there were two broadly

different composite structures, one for low AC content (1_AC/TiO₂ to 15_AC/TiO₂) and one for high AC content (30 AC/TiO₂ and 75_AC/TiO₂).

The homogeneity of the powder particle composition was analyzed using KEVEX Si(Li) Brüker software-assisted EDS in the SEM. The aim of this characterization was not to provide quantitative analysis but rather to assess the homogeneity of the synthesized powder, as carbon is hard to quantify in our device configuration. Although the depth resolution of each EDS analysis is dependent on the sample nature and the electron beam energy, it was estimated that the depth resolution ranges from less than one micrometer to few micrometers for a 5kV low electron beam energy [47], allowing us to assume that only one or a few particles are taken into account for a local EDS analysis. We thus carried out 10 analyses at different points of each powder and reported the average composition values with standard deviations in Table 1. The compilation of elemental analysis data for each sample revealed that: (i) average composition values calculated from 10 local analyses were close to the original AC/TiO₂ ratios for all composite samples; (ii) standard deviations calculated from these measures were less than 8% for each component's weight percentage value. Thus, for each composite sample, the elemental analysis is repeatable through the whole powder and even for very small analytical sample volumes. We can thus assert that powder aggregates of all the studied AC/TiO₂ samples present a degree of compositional homogeneity in addition to the previously-highlighted size-distribution homogeneity.

The particle-size homogeneity of the composite powders was analyzed using an image processing protocol. First, 0.01g of AC/TiO₂ powder was added to 10 mL acetone and sonicated for 15 min to obtain a dispersed suspension and break up the agglomerates. A few drops of the suspension were deposited onto a silica substrate and left to air-dry for 1 min, leading to dispersed composite particles on the silica substrate. SEM images were then taken at low magnification ($\times 3000$) to allow granulometric analysis of the composite powders by digital image processing at a sufficient resolution to be able to detect any submicron-sized (>100 nm) particles. Note that for all images taken at this magnification (Fig. 1), there were more than a few dozen per image. To make granulometric analysis possible, we took a hundred images in order to reach at least 1000 particles for a sufficiently representative granulometric analysis [48]. All these images were processed using the open-source program ImageJ as follows: (i) image binarization to detect the particle edges and thus obtain the particle surface areas; (ii) calculation of the equivalent spherical diameters from the particle surface areas.

This image processing protocol was conducted to characterize sample granulometries for all the composites by computing particle volume density as a function of particle diameter (Fig. 2). As the 10h milling time was chosen, composites milled for a shorter time (1h) were reported on each composite granulometric analysis to verify the particle size convergence from a chaotic distribution to a clean Gaussian [43].

All 1h-milled samples displayed size distributions between 0.5 and 15 μm , showing the size-reducing effect of mechanosynthesis on introduced particles as small as a few dozen microns. The 1h-milled samples did not show size distribution homogeneity nor trends as a function of composition. However, an increase of milling time to 10h reduced the width of the size distribution as well as the size distribution heterogeneity. All samples synthesized within the scope of this work (1_AC/TiO₂ to 75_AC/TiO₂) exhibited a monomodal particle size distribution which looks like a Gaussian function. We therefore used a Gaussian probability density function (eq. (1)) to fit the experimental measured particle distributions of these composite powders:

$$f(x) = \frac{1}{\sigma\sqrt{2\pi}} e^{-\frac{1}{2}\left(\frac{x-\mu}{\sigma}\right)^2} \quad (1)$$

where x is particle diameter, μ is the mean size distribution value, and σ is the standard deviation. For each sample, the mean particle diameter found was around $3.1 \pm 0.4 \mu\text{m}$ and the standard deviation was 1.00 ± 0.15 (Table 2). Note that R^2 , the correlation coefficient between experimental granulometry and theoretical representation by a Gaussian function, was always superior to 0.97. This last investigation allowed us to highlight that the chosen 10h mechanosynthesis protocol leads to a tight Gaussian-like particle size distribution centered around 3 μm , independently of the initial AC/TiO₂ composition.

3. Results

3.1. Experimental conditions

Adsorption and photodegradation batch experiments were carried out using 100 mL caffeine solutions produced with ultrapure water (18 M Ω) and reagent plus-grade caffeine powder (>99.0% purity) purchased from Sigma-Aldrich USA. This molecule was chosen as a target of adsorption and photodegradation as it is recalcitrant to classical water treatment processes [49] and safer to handle than a lot of emerging bio-recalcitrant molecules [50].

Caffeine concentration was followed over time via ultra-high-performance liquid chromatography using an Ultimate 3000 Thermo Scientific system equipped with a UV-Vis detector and a C-18 Hypersil GOLD column (100 mm x 2.1 mm; particle size: 5 μm). Isocratic elution mode with detection at $\lambda = 274 \text{ nm}$ was used with an initial 90:10 (v/v) water:acetonitrile mixture at a $0.6 \text{ mL}\cdot\text{min}^{-1}$ flowrate. A 40W neon source whose spectrum is centered at 370 nm was placed above the testbench at a distance set to give an average incident flux density on beaker solutions of $25 \text{ W}\cdot\text{m}^{-2}$. The irradiation source was shut off for adsorption runs and turned on for photocatalytic degradation experiments.

3.2. Adsorption capacity

First we investigated the adsorption capacity of the composites in order to study the effect of composition. Sample preparation for adsorption measurements was as follows. The amount of powder put in the caffeine solution was chosen as 0.1 g. Powders were then put in solutions containing different initial concentrations of caffeine and then magnetically stirred for enough time to reach an equilibrium of caffeine between liquid phase and solid phase. The adsorption capacity of each powder was then obtained from these equilibria by plotting adsorbed caffeine in mg/g of powder against liquid-phase balance concentration ($\text{mg}\cdot\text{L}^{-1}$). Here we chose to represent the adsorbed caffeine amount per gram of powder instead of representing it per gram of adsorbent material in order to depict the real adsorption capacity of each composite powder considering them as new entities. To do so, all experiments were stopped once variation of the liquid-phase caffeine concentration lower than $2 \text{ mg}\cdot\text{L}^{-1}$ over 5h. This choice emerged from a previous work where a limit criterion of $0.4 \text{ mg}\cdot\text{L}^{-1}\cdot\text{h}^{-1}$ was defined [18], and is assumed to be adapted for our experiments since the criterion value is low compared to the total caffeine concentration divided between the liquid and solid phases.

Adsorption isotherms were fitted using Langmuir isotherm theory, based on the assumption that adsorption occurs in a continuous monolayer on a homogeneous surface [51]. This model was found to be consistent with the AC adsorption mechanism, which is characterized by monolayer adsorption on the material micropores, as confirmed by the type-I shape (IUPAC classification) of its isotherm [18,43]. Langmuir's isotherm model is represented by the following equation (2):

$$q_e = \frac{q_{\max} b C_e}{1 + b C_e} \quad (2)$$

where q_e is amount adsorbed at equilibrium ($\text{mg}\cdot\text{g}^{-1}$), q_{max} is a constant representing the maximum adsorption capacity of the adsorbent ($\text{mg}\cdot\text{g}^{-1}$), b is a constant that depicts the energy of adsorption and is related to adsorbent/adsorbate affinity ($\text{L}\cdot\text{mg}^{-1}$), and C_e is liquid-phase concentration at equilibrium ($\text{mg}\cdot\text{L}^{-1}$). Fitting all samples with this model enabled us to obtain q_{max} and b constants for each. These parameters are summarized in Table 3.

As expected, M_{TiO_2} had the lowest adsorption capacity (Fig.3.A), which was almost null even at high caffeine concentration in the liquid phase. Conversely, the adsorption capacity of raw unmilled AC was plotted as a reference and exhibited the highest adsorption capacity, characterized by a high coefficient slope at low equilibrium concentration (i.e. 0-50 $\text{mg}\cdot\text{L}^{-1}$) and a saturation plateau at higher concentrations for which adsorbed caffeine amount was around $395 \text{ mg}\cdot\text{g}^{-1}$. As expected, all other powder adsorption curves were midway between raw AC and raw TiO_2 . Comparison between composite samples showed that adsorption capacity increased with increasing AC content.

Adsorption capacity decreased from raw unmilled AC down to the milled AC for which both slope and saturation plateau were lower than the unmilled powder. Indeed, the saturation plateau for the M_{AC} isotherm corresponds to an adsorbed caffeine quantity of about $245 \text{ mg}\cdot\text{g}^{-1}$, which represents 60% of the amount of the unmilled AC plateau. This difference is related to the mechanical milling process which altered part of the AC adsorption capacity by degrading part of its porous structure. This assumption was verified through nitrogen adsorption isotherm at 77 K using a Micromeritic Tristar II 3020 analyzer on both milled and unmilled AC. This test revealed that unmilled AC BET surface area and micropore area were respectively as high as $1742 \text{ m}^2/\text{g}$ and $767 \text{ m}^2/\text{g}$ and falls to $1022 \text{ m}^2/\text{g}$ and $619 \text{ m}^2/\text{g}$ when the AC was milled. This assertion is also consistent with what was observed for dry-milled AC in previous works [52].

AC/TiO_2 composites presented adsorption capacity profiles situated between the two pure component curves. Indeed, compared with pure AC powder, they have lower but partially preserved adsorption capacity, which in terms of saturation plateau was close to M_{AC} with $75_{\text{AC}}/\text{TiO}_2$ and close to an adsorbed amount of $5 \text{ mg}\cdot\text{g}^{-1}$ with $1_{\text{AC}}/\text{TiO}_2$. The extracted Langmuir constant, b , for all samples was relatively low (Table 3) and consistent with a low binding energy of AC with caffeine [49], and more generally with the physical and thus reversible adsorptive behavior of an AC/adsorbate pair when b is low [53]. If we compare the extracted composite constant q_{max} against to M_{AC} as a reference sample, the maximum adsorbed amount represents around 92% of the reference sample for the $75_{\text{AC}}/\text{TiO}_2$

composite. This maximum capacity decreases with increasing TiO₂ content in the composite, reaching a relative value as low as 1% of the sample reference for the 1_AC/TiO₂ powder. As expected, the maximum adsorbed quantity q_{\max} is mainly dependent on AC amount in the composite. However, it can be pointed out that the proportionality factor is not fully respected along composition, suggesting that the mechanosynthesis history was different on each composite.

3.3. Sorption rate

The sorption process can be described as a transfer of adsorbate molecules from liquid phase to solid phase. Sorption kinetics thus describe the kinetics of adsorbate transfer from the solution to the adsorbent surface, which is dependent on the adsorbent/adsorbate affinity characterized earlier, and is also limited by two phenomena: (i) diffusion occurring in the liquid layer at the adsorbent/water interface, and (ii) intraparticle mass transfer. The aim was then to study the effect of composition on the transfer kinetics of AC/TiO₂ composites. Sorption transfer kinetics were assessed following almost the same routine as that used to compute sorption capacity, the only difference in the protocol being that we tracked the time-course of the adsorption mechanism by analyzing caffeine concentration at regular intervals until equilibrium was reached. We consequently selected a different initial caffeine concentration for each sample, the goal being to reach the same equilibrium on the isotherm plateau ($C_e = 200 \text{ mg.L}^{-1}$) for each composite. For each analyzed powder, 6 adsorption experiments were made with the same selected initial concentration. The time measure started when the sample was put in the solution. Caffeine concentration analysis was performed only once at the end of each of the adsorption experiments, which were stopped at different times, i.e.: 1, 5, 30, 60, 120, and 180 min. We thus achieved adequate precision and repeatability, as it is well-known that making many solutions and only taking one sample on each prevents the risk of creating the large analytical biases (by withdrawing solution volume and/or adsorbent material throughout the experiment) that can appear while repeatedly taking samples from the same one solution.

The linear driving force (LDF) model for adsorption kinetics considers the two phenomena that limit adsorption, i.e. diffusion at the solid/liquid interface and intraparticle transfers. This formalism is commonly used to describe microporous adsorbent transfer kinetics [20,54-56]. Under this model, the adsorbate balance between liquid phase and solid phase is expressed with the following differential equations (3) and (4):

$$\frac{dC_t}{dt} = -k_{ads}C_{samp}(q_e - q_t) \quad (3)$$

$$\frac{dq_t}{dt} = k_{ads}(q_e - q_t) \quad (4)$$

where C_t is caffeine concentration in the solution at time t (g.L^{-1}), k_{ads} is the transfer coefficient (s^{-1}), C_{samp} is sample (AC, TiO_2 or Composite) concentration in the solution (g.L^{-1}), q_e is the amount of adsorbate adsorbed at equilibrium (mg.g^{-1}), and q_t is the amount of caffeine adsorbed at time t (mg.g^{-1}). By solving this system of differential equations (eq. (3) and (4)), we can obtain a concentration profile in the liquid and solid phases over time and assess the k_{ads} constant.

All sample concentration profiles on the composites were reported over time (Fig. 4). As expected, pure M_AC and M_ TiO_2 exhibited opposite behaviors in terms of adsorption kinetics: maximal adsorption capacity and transfer kinetics constants were obtained for M_AC whereas the lowest adsorbed amount and transfer speeds observed across all the samples studied were for M_ TiO_2 . Indeed, the transfer coefficient was extremely low as $0.4 \times 10^{-4} \text{ s}^{-1}$ for M_ TiO_2 while the constant computed for M_AC was almost 100 times higher ($34.29 \times 10^{-4} \text{ s}^{-1}$) (Table 3). Note that caffeine adsorption occurred faster for AC/ TiO_2 composites than for M_ TiO_2 but still slower than for M_AC powder. Note too that the transfer kinetic constants for composite samples increased with increasing carbon content, but this trend was not directly proportional to AC/ TiO_2 composition: indeed, the kinetic constant computed for 15_AC/ TiO_2 composite was $16.6 \times 10^{-4} \text{ s}^{-1}$, which is almost half of the value computed for 75_AC/ TiO_2 ($32.1 \times 10^{-4} \text{ s}^{-1}$) whereas 75_AC/ TiO_2 has five times more AC. Anyway, whatever the composition, the simple LDF model made it possible to have a rather good estimation of the sorption kinetic.

3.4. Photodegradation kinetics

In order to quantify the capacity of the studied composites to photo-oxidize caffeine in solution, it is obviously necessary to separate photodegradation from removal by adsorption. We therefore began the photodegradation experiments with an adsorption phase (UV lamp off) which was chosen to last 180 min in line with the stop criterion defined in section 3.2 for the adsorption isotherm. The experiments were designed to meet requirements on (i) the amount of composite powder quantity selected for the experiment and (ii) the initial caffeine concentration. We made the choice to compare the performance of the composites in photo-

oxidation on the basis of a same amount of TiO₂ whatever is the material composition. Previous work had defined 2 g.L⁻¹ TiO₂ as the amount of Aeroperl® P25 to absorb the major part of the light (more than 90% of the incident light density is absorbed) in conditions similar to our experimental system (0.02 m of suspension crossed by near-UV light) [57]. A TiO₂ content of 0.2 g was thus our criterion defining the mass of each composite powder added in the caffeine solution.

Experimental conditions were selected in term of caffeine concentration within the objective to qualify and quantify the photo-oxidation rate without any interaction or coupling with sorption phenomena. The most favorable conditions to reach this objective were: (i) to provide photo-oxidation with composites initially saturated in caffeine ($q_{eq} \approx q_{max}$); (ii) to carry the photodegradation process for each composite without any change in the adsorbed caffeine amount in AC. In practice, such a working mode needed to stop photo-oxidation once a caffeine concentration in the liquid phase of 100 mg/L was reached (Fig. 3). Additionally and ideally, the initial concentration when the photo-oxidation started had to be the same for each experiment. To meet these requirements, a preliminary phase of adsorption was systematically carried out with an initial caffeine concentration adapted to each composite as indicated on Figure 5.A. After this preliminary phase running from 0 to 180 min, UV lamp was turned on.

The relative caffeine concentration plot was built from the photodegradation phase (Fig. 5.A) to focus on the photocatalytic activity of each sample (Fig. 5.B.). M_TiO₂ exhibited the best photodegradative behavior against caffeine whereas M_AC had, as expected, no photocatalytic activities. Regarding composite responses, composite photocatalytic activity increased with decreasing AC contents. Note too that for all powders, the change in caffeine concentration looks constant over time. This trend is in good agreement with experimental conditions free from diffusion by mass transfer where the reaction rate is maximum [58]. The linear time-course curve of caffeine concentration can be described using a zero-order kinetic model described by equation (5):

$$\frac{dC_t}{dt} = -\alpha_{app} \quad (5)$$

where C_t is caffeine concentration in the solution at time t (mg.L⁻¹), and α_{app} is the apparent photodegradation kinetic constant (mg.L⁻¹.s⁻¹).

The zero-order kinetic law fits well with experimental results (Fig. 5.B). Apparent photodegradation constants were extracted for each powder and reported in Table 3. The

maximum photodegradation constant value obtained for M_TiO₂ was $14.1 \times 10^{-3} \text{ mg.L}^{-1}.\text{s}^{-1}$ whereas M_AC had a null α_{app} value. Regarding composite responses, composite photocatalytic activity decreased with increasing AC contents. As seen earlier, the photo-oxidative properties of the composites did not evolve linearly with composition. Indeed, the apparent photodegradation constant for 75_AC/TiO₂, 30_AC/TiO₂ and 15_AC/TiO₂ were in the range $0.73\text{--}3.91 \times 10^{-3} \text{ mg.L}^{-1}.\text{s}^{-1}$ which is 3 to 5 times lower than the constant measured for M_TiO₂. The two composites with higher TiO₂ contents, i.e. 5_AC/TiO₂ and 1_AC/TiO₂, showed much better photocatalytic degradation capacity. The α_{app} constant of 5_AC/TiO₂ and 1_AC/TiO₂ were consistent with this observation, at 6.41 and $8.91 \times 10^{-3} \text{ mg.L}^{-1}.\text{s}^{-1}$ for 5_AC/TiO₂ and 1_AC/TiO₂, respectively. Note that the highest composite constant value was almost half of the value obtained for M_TiO₂. Thus, adding a small amount of AC with TiO₂ for mechanosynthesis partially inhibited the photocatalyst's degradation capacity.

4. Discussion

This section sets out to understand the phenomena involved and define how far composition shapes the functional properties of the composites, i.e. photo-oxidation rate, efficiency and sorption properties (isotherm and rate) for a solar photo-oxidation application.

4.1. Properties correlation

In the context of a photo-oxidation treatment application, it is necessary to define the properties according to the constraints and uses imposed. Here, mechanical synthesis makes it possible to modify the composition of AC/TiO₂ composites in order to modulate their functional properties. These functional properties, previously determined for different AC/TiO₂ compositions, are shown in Figure 6 according to the mass ratio of AC.

The parameters q_{max} and b are characteristic of the adsorbent properties of composites [59]. As expected, the maximum amount adsorbed, i.e. q_{max} derived from eq. (2), varies drastically according to composition in the field studied. While this characteristic is close to zero for the catalyst alone, it increases when increasing AC ratio, reaching a maximum value with pure AC. As shown in Figure 6, the mechanosynthesis process alters the adsorbent properties of the AC within the composite, but this alteration does not seem to be correlated to composition. In other words, the presence of TiO₂ in the composite does not limit the accessibility of molecules to the microporous network of AC, regardless of the materials composition. As shown by results

reported in Figures 3 and 6, this implies that the adsorption capacities mostly on the amount of AC in the composite.

The coefficient k , determined by the system of eq. (3) and (4), reflects the rate of transfer of molecules from liquid to adsorbed phase, in this case from the solution to the catalyst pore surface. The variation of this coefficient, as reported in Figure 6 as a function of composition, highlights two points. First of all, the transfer rate is highly dependent on the nature of the selected material [14-15]. Indeed, the k coefficient was more than 10 times higher for AC than for catalyst (Table 3). The higher adsorption kinetic of AC is explained by the microporous network developed by the material which generates a very high adsorption capacity ($q_{\max}=300\text{mg/g}_{ca}$). It is likely that its adsorption capacity induces a high concentration gradient at the solution/composite interface, and is thus the driving force behind the material transfer. In comparison, the catalyst alone has a particularly low transfer coefficient. This second observation is tied to the fact that the coefficient does not vary linearly according to composition. Whatever the composition, it was higher than the average value weighted by AC composition. It should be kept in mind that Q_{\max} variation with composition highlighted that TiO_2 does not block the adsorption on AC within the composite structure. However, the observation of the change in Langmuir affinity constant b among composition show that it has its highest value for catalyst alone and decreases while AC amount is increased, allowing us to assert that caffeine molecule has a better affinity with TiO_2 than with AC. These two observations led us to correlate the k_{ads} kinetic constant change with composition to these properties, asserting that the TiO_2 , having a better affinity with caffeine molecules, is slowing the transfer mechanism from the solution to the AC adsorption sites within the composites. Thus, correlating these adsorption properties all together highlight that no synergy is observed between the catalyst and the adsorbent from an adsorption perspective.

Focusing on the effect of composition on oxidative kinetics, we noted that the behavior of composites highlights two factors. At low AC wt%, the oxidative kinetic decreases significantly up to the 30_AC/ TiO_2 composite but then shows less marked variation at higher compositions. For comparison, the photo-oxidation constant decreases by a factor of 3 in the 30-75 AC wt% range but decreases by a factor of 7 in the 0 to 30 AC wt% range. The presence of AC, even in small quantities, strongly degrades the catalytic properties of the composites: inserting just 1% carbon by mass induces a 50% loss of photodegradation kinetic. It is possible that the presence of even small quantities of carbon on composite surface significantly modifies its optical properties. Indeed, the optical properties of carbon make it particularly absorbent and poorly

reflective over the spectral range considered [60,61]. The consequence is a direct loss in terms of photons available to activate the photo-excitation mechanism on the catalyst surface. This phenomenon engages a cascading effect that limits the production of radical species and therefore reduces the oxidative kinetic of the in-composite catalyst.

These patterns, which reveal a non-linear evolution of the functional properties of composites as a function of composition, are well-established specificities of granular materials [62-64]. By highlighting the non-linearity of the properties and behavior of granular materials, these studies revealed ruptures in singular compositions called ‘percolation thresholds’ [63]. For example, the optical and electrical properties of grain mixtures (insulator/conductor) show non-linear changes in singular composites 30_AC/TiO₂ and 75_AC/TiO₂ [65,66]. On the domains delimited by these points, the properties are either stable or vary linearly. These particularities are explained by key characteristics of granular materials such as size, grain size distribution and size ratio and/or key properties of the entities making up the granular composite, such as optical, electrical, radiative and mechanical characteristics [65,66].

4.2. Photocatalytic efficiency

In the field of advanced oxidation processes, the performance of photocatalytic materials is evaluated by rate or kinetic of photodegradation [27,67,68]. Many authors have used radical formation as a reference measurement for photocatalytic activity, but these approaches are dependent on the operating conditions (pH, water composition) and the conditions applied (flow density, concentration) [69]. To assess the photocatalytic performance of a system for comparison independently of experimental conditions, photochemists have introduced the concept of photonic efficiency. Photonic efficiency is a yield defined by the number of radicals produced per absorbed photon and characterized by the primary photoelectric excitation mechanism initiated by a perfectly homogeneously-solubilized catalyst in solution [70]. But in polyphasic systems, as is the case with heterogeneous photocatalysis, photonic efficiency does not consider the phenomenon of radiative and mass transfers at the interfaces of liquid and solid phases [71,72]. Serpone et al. therefore introduced photocatalytic efficiency, η , to evaluate the capacity of photocatalysts in solid form, where η is number of molecules photo-converted per unit volume of solution divided by the number of photons absorbed on the surface of the catalyst [71,73-75]:

$$\eta = \frac{N_A \cdot V \cdot \Delta C_t}{S \int_{\lambda_1}^{\lambda_2} \int_0^t I(t) dt} \quad (7)$$

where C_t is concentration of the molecules at a time t , V is volume of the cell (m^3), N_A is Avogadro number (mol^{-1}), S is irradiated surface (m^2), and I is flux density of photons (photon number. $\text{m}^{-2}.\text{s}^{-1}$).

For this study, we determined the photocatalytic efficiency of composites prepared at different AC/catalyst compositions. Number of photo-converted molecules was derived from experimental measurements of variation in caffeine concentration as a function of irradiation time. Thus, potential byproducts resulting from caffeine degradation were there neglected. Number of photons was calculated from the characteristics of the lamp emitting the UV radiation, i.e. its spectral distribution, its spectral range, and duration of the irradiation. These conditions, which were established in previous work, made it possible to assess the flux density of photons [76,77]. These quantities are shown in Figure 7a on the x -axis and y -axis, respectively. The data for each composite was linearly fitted by a straight line that passes through the origin and whose slope gives the photocatalytic efficiency of the composite concerned (eq. (7)). The highest efficiency, which reached 0.6%, was found for the catalyst alone, and was of the same order of magnitude as that obtained in the literature for TiO_2 suspensions in nanometric and micrometric powder forms [76-79]. For the composites, photocatalytic efficiency decreased as the proportion of carbon increased, from pure catalyst down to pure AC which has zero photocatalytic activity. Photocatalytic efficiency varied from 0.4% for the 1% carbon composite (1_AC/ TiO_2) to less than 0.04% for a predominantly carbon composite (75_AC/ TiO_2). By studying these composites under particular conditions, i.e. at very high concentrations of target molecules so that the mass transfer is not limiting, our results focused on the photocatalytic kinetic of composites by emerging the effect of composition independently of the other parameters. The advantage of this approach was to be able to scan the entire composition spectrum while using the same one method and maintaining the same composite preparation conditions.

The efficiencies reported in Figure 7a are expressed as a function of number of photons absorbed by the composite without discriminating between the photons absorbed by the AC—and therefore lost for photo-excitation—and those reaching the catalyst surface that could potentially initiate the photo-excitation mechanism. To assess and compare the efficiency of

the catalyst, whether alone or within the composite, it is proposed to consider only the proportion of photons absorbed by the catalyst, i.e. photons that are potentially effective for the production of radicals. Figure 7b thus charts the number of photo-converted as a function of number of effective photons, which is there assumed to correspond to the number of incident photons multiplied by the catalyst volume fraction of the composite. This representation, although simplifying the light management within the suspension, allowed to highlights two points. On one hand, the catalyst alone develops the greatest efficiency, thus emphasizing that TiO₂ used as a pure compound is more efficient than TiO₂ within a composite. In other words, the presence of AC in the catalyst environment limits its photocatalytic kinetic. Contrary to reports in the literature, this result tends to prove that there is no synergy related to the coupling of AC with a catalyst. Indeed, some studies suggest that the concentration of molecules on an adsorbent near the catalyst intensifies the photocatalytic kinetic of the catalyst [25, 30, 32]. Other studies indicate that AC promotes the transfer of molecules to the catalyst surface. Under these conditions, the diffusion of in-solution molecules towards the catalyst surface is no longer limiting, and so the photo-degradation rate is increased [17,28,29, 31-33]. The second reason this representation is informative is that the composites all develop the same efficiency, which tends towards 0.04%, regardless of their AC fraction, In other words, the intrinsic photocatalytic efficiency of TiO₂ does not appear to be altered or intensified by variation in the amount of AC in its close environment. This implies that the mechanisms of photo-excitation and radical production in the composite-integrated catalyst are independent of the AC fraction.

Conclusion

The first aim of this work was to control functional properties of AC/TiO₂ composites, i.e. sorptive capacity, mass transfer, and photocatalytic activity. Pollutant storage, AC regeneration and photo-oxidation improvement are the targeted applications these focal functional properties need to be modulated by modifying the composition of AC/TiO₂ composites. This was done by controlling adsorbent/catalyst ratio at the initial stage of the synthesis. Mechano-synthesis was chosen as a novel method for preparing adsorbents associated with photocatalysts. Using this method, we successfully synthesized composites covering the entire range of possible compositions presented in the first part of this work. The as-made composite powders were shown to be homogeneous and repeatable.

The second part of this work consisted in studying the functional properties of all the synthesized AC/TiO₂ composites. The study on the sorption capacity of the powders highlighted that mechanosynthesis partially altered AC adsorption capacity. However, this alteration was independent to the composition of the AC/TiO₂ powder. Furthermore, the results of the mass transfer study revealed that although TiO₂ presence was not affecting the adsorption capacity of the composites, it affects significantly the transfer kinetic. Indeed, an augmentation of TiO₂ amount in the composite induces a decrease of the transfer kinetic. On the other hand, we found that the photo-oxidation property was composition- dependent. Indeed, photodegradation kinetic increases with increasing TiO₂ ratio in the AC/TiO₂ powder.

We completed this study with a discussion around the behavior of the composites, and a photonic efficiency study. The composites mechanisms involved in the composites' functional properties were investigated and both the synthesis history and catalyst/adsorbent interactions were used as arguments to explain the patterns of change in sorption and photodegradation properties as a function of composition. The photonic efficiency study found that raw TiO₂ powder exhibits higher efficiency than TiO₂ composites. This observation underlined that there is no synergy between AC and TiO₂. However, we also found that TiO₂ efficiency in composites was almost constant whatever the composition, thus demonstrating that the photo-oxidation mechanism operates independently of any AC in the catalyst's close environment.

We ultimately found that the composite characteristics captured through this study are not all proportional to composition. This effect is an interesting highlight from an applications perspective, as it paves the way to selecting the best AC/TiO₂ composition for a given target application, for instance (i) high-adsorption-capacity composites for pollutant storage applications and (ii) intermediate adsorption and photocatalytic properties for pollutant storage/filter regeneration applications.

Acknowledgements

This work has been supported by the Occitanie Region in France and by European Regional Development Fund (ERDF) provided by the European Union.

References

- [1] D.Y. Goswami, F. Kreith, J.F. Kreider, 1999, "Principles of solar engineering", 2nd Edition, Taylors & Francis Co., Philadelphia.
- [2] JA. Duffie, WA. Beckman, 2013, "Solar engineering of thermal processes, Fourth Edition", John Wiley and sons Inc.
- [3] A. Kéré, V. Goetz, X. Py, R. Olives, N. Sadiki, 2015, "Modeling and integration of a heat storage tank in a compressed air electricity storage process", *Energy Conversion and Management* 103, 499-510.
- [4] J. -F. Hoffmann, T. Fasquelle, V. Goetz, X. Py , 2016, "A thermocline thermal energy storage system with filler materials for concentrated solar power plants: Experimental data and numerical model sensitivity to different experimental tank scales", *Applied Thermal Engineering* 100, 753-761.
- [5] J. -F. Hoffmann, T. Fasquelle, V. Goetz, X. Py, 2017, "Experimental and numerical investigation of a thermocline thermal energy storage tank", *Applied Thermal Engineering* 114, 896-904.
- [6] S. Malato, J. Blanco, A. Vidal, C. Richter, 2002, "Photocatalysis with solar energy at a pilot-plant scale: an overview", *Applied Catalysis B: Environmental* 37, 1-15.
- [7] J. Galvez and S. Malato, 2003, "Solar Detoxification", United Nations Educational, Scientific and Cultural Organization.
- [8] O. Schmidt, S. Melchior, A. Hawkes and I. Staffell, 2019, "Projecting the Future Levelized Cost of Electricity Storage Technologies", *Joule* 3, 81-100.
- [9] D. Haillot, S. Pincemin, V. Goetz, D.R. Rousse, X. Py, 2017, "Synthesis and characterization of multifunctional energy composite: Solar absorber and latent heat storage material of high thermal conductivity" , *Solar Energy Materials and Solar Cells* 161, 270-277.
- [10] C. Minero, 1999, "Kinetic analysis of photoinduced reactions at the water semiconductor interface", *Catalysis Today* 54, 205-216.
- [11] J.M. Herrmann, 1995, "Heterogeneous photocatalysis: an emerging discipline involving multiphase system", *Catalysis today* 24, 157-164.
- [12] A.G. Agrios and P. Pichat, 2005, "State of the art and perspectives on materials and applications of photocatalysis over TiO₂", *Reviews in applied Electrochemistry* 58.
- [13] S. Malato, J. Blanco, A. Campos, J. Caceres, C. Guillard, J.M. Herrmann, A.R. Fernandez-Alba, 2003, "Effect of operating parameters on the testing of new industrial titania catalysts at solar pilot plant scale", *Applied Catalysis B: Environmental* 42, 342-357.

- [14] C.T. Chekem, Y. Richardson, M. Drobeck, G. Plantard, J. Blin and V. Goetz, 2017, "Effective coupling of phenol adsorption and photodegradation at the surface of micro and mesoporous TiO₂ activated carbon", *Reaction Kinetics, Mechanisms and Catalysis* 122 (2), 1297-1321.
- [15] C.T. Chekem, V. Goetz, Y. Richardson, G. Plantard, J. Blin, 2019, "Modeling of adsorption/photodegradation phenomena on CA-TiO₂ composites catalyst for water detoxification", *Catalysis Today* 328, 183-188.
- [16] W. Jo, S. Shin, E.S. Hwang, 2011, "Removal of dimethyl sulfide utilizing activated carbon fiber-supported photocatalyst in continuous-flow system", *Journal of Hazardous Materials* 191, 234-239.
- [17] J. Matos, J. Laine, J.-M. Herrmann, D. Uzcategui, J.L. Brito, 2007, "Influence of activated carbon upon titania on aqueous photocatalytic consecutive runs of phenol photodegradation", *Applied Catalysis B: Environmental* 70, 461-469.
- [18] M. Miguet, V. Goetz, G. Plantard, Y. Jaeger, 2015, "Removal of a chlorinated volatile organic compound from aqueous phase by adsorption on activated carbon", *Industrial and Engineering Chemistry Research* 54, 9813-9823.
- [19] M. Miguet, V. Goetz, G. Plantard, Y. Jaeger, 2016, "Sustainable thermal regeneration of spent activated carbons by solar energy: application to water treatment", *Industrial and Engineering Chemistry Research* 55 (25), 7003-7011.
- [20] V. Goetz, T. Janin, G. Plantard, S. Brosillon, 2013, "Hybridation between heterogeneous photocatalysis and adsorption", *International journal of Engineering practical research* 2 (3), 86-93.
- [21] G. Plantard, A. Azais, J. Mendret, S. Brosillon, V. Goetz, 2018, "Coupling of photocatalytic and separation processes as a contribution to mineralization of wastewater", *Chemical Eng. And Processing: Process intensification* 134, 115-123.
- [22] N. Areerachakul, S. Vigneswaran, H.H. Ngo, J. Kandasamy, 2007, "Granular activated carbon (GAC) adsorption-photocatalysis hybrid system in the removal of herbicide from water", *Separation and Purification Technology* 55, 206-211
- [23] P. Atheba, D. Robert, A. Trokourey, D. Bamba, J.-V. Weber, 2009, "Design and study of a cost-effective solar photoreactor for pesticide removal from water", *Water Sci. Technol.* 60, 2187-2193.
- [24] J.C. Critenden, P.S.S. Rominder, D.L. Perram, D.W. Hand, 1997, "Decomtamination of water using adsorption and photocatalysis", *Wat. Res.* 31 (3), 411-418.

- [25] E.F. Mohamed, 2011, "Removal of organic compounds from water by adsorption and photocatalytic oxidation", INPT, University of Toulouse.
- [26] C. Chekem, 2017, "Matériaux carbonés multifonctionnels à porosité contrôlée à partir des ressources végétales tropicales : application au traitement de l'eau par photocatalyse", Thèse de doctorat Université de Perpignan Via Domitia.
- [27] J.M. Herrmann, J. Matos, J. Disdier, C. Guillard, J. Laine, S. Malato, J. Blanco, 1999, "Solar photocatalytic degradation of 4-chlorophenol using the synergistic effect between titania and activated carbon in aqueous suspension", *Cat. Tod.* 54 (2-3), 255-265.
- [28] Matos J., Laine J., Herrmann J.-M. (1998) Synergy effect in the photocatalytic degradation of phenol on a suspended mixture of titania and activated carbon, *Applied Catalysis B: Environmental* 18, 281-291
- [29] G. Xue, H. Liu, Q. Chen, C. Hills, M. Tyrer, F. Innocent, 2011, "Synergy between surface adsorption and photocatalysis during degradation of humic acid on TiO₂/activated carbon composites", *Journal of Hazardous Materials* 186 (1), 765-772.
- [30] X. Zhang, M. Zhou, L. Lei, 2005, "Enhancing the concentration of TiO₂ photocatalyst on the external surface of activated carbon by MOCVD", *Materials Research Bulletin* 40 (11), 1899-1904.
- [31] N.G. Asenjo, R. Santamaria, C. Blanco, M. Granda, P. Alvarez, R. Menendez, 2013, "Correct use of the Langmuir–Hinshelwood equation for proving the absence of a synergy effect in the photocatalytic degradation of phenol on a suspended mixture of titania and activated carbon", *carbon* 55, 62-69.
- [32] K. Baransi, Y. Dubowski, I. Sabbah, 2012, "Synergetic effect between photocatalytic degradation and adsorption processes on the removal of phenolic compounds from olive mill wastewater", *Wat. Res.* 46 (3), 789-798.
- [33] W. Wei, C. Yu, Q. Zhao, X. Qian, G. Li, Y. Wan, 2014, "Synergy effect in photodegradation of contaminants from water using ordered mesoporous carbon-based titania catalyst", *Applied Catalysis B: Environmental* 146, 151-161.
- [34] B. Cagnon, 2002, "Elaboration de charbons actifs à texture contrôlée", Thèse de doctorat Université de Perpignan Via Domitia.
- [35] B. Cagnon, X. Py, A. Guillot, F. Stoeckli, 2005, "The effect of the carbonization/activation procedure on the microporous texture of the subsequent chars and active carbons", *Microporous and Mesoporous Materials* 80, 183-193.

- [36] R. Yuan, R. Guan, J. Zheng, 2005, "Effect of the pore size of TiO₂-loaded activated carbon fiber on its photocatalytic activity", *Scripta Materialia* 52 (12), 1329-1334.
- [37] X. Py, V. Goetz, G. Plantard, 2008, "Activated carbons textural optimization for gas storage processes", *Chemical Engineering and Processing: Process intensification* 47 (3), 308-315.
- [38] A. Bhatnagar, W. Hogland, M. Marques, M. Sillanpää, An overview of the modification methods of activated carbon for its water treatment applications, *Chem. Eng. J.* 219 (2013) 499–511.
- [39] R. Leary, A. Westwood, 2010, "Carbonaceous nanomaterials for the enhancement of TiO₂ photocatalysis", *Carbon* 49 (3), 741-772.
- [40] S. Seifried, M. Winterer, H. Hahn, 2000, "Nanocrystalline Titania films and particles by chemical vapor synthesis", *Chem. Vap. Deposition* 6, 239-244.
- [41] A.I. Martinez, D. R. Acosta, A.A. Lopez, 2004, "Effect of deposition methods on the properties of photocatalytic TiO₂ thin films prepared by spray pyrolysis and magnetron sputtering. *J. Phys.: Condens. Matter* 16 (22), 2335-2344.
- [42] J. Matos, M. Hofman, R. Pietrzak, 2013, "Synergy effect in the photocatalytic degradation of methylene blue on a₂ and N-containing carbons", *Carbon* 54, 460-471.
- [43] E. Ribeiro, V. Goetz, F. Teyssandier, F. Maury, N. Sadiki, D. Chaumont, G. Plantard, Mechanosynthesis as new method for Activated-Carbon/TiO₂ composites preparation: feasibility and Sorption/Photodegradation capabilities, *applied catalysis* (unpublished).
- [44] C. Suryanarayana, 2001, "Mechanical alloying and milling", *Progress in Materials Science* 46, 1-184.
- [45] J. Carbajo, A. Tolosana-Moranchel, J.A. Casas, M. Faraldos, A. Bahamonde, 2018, "Analysis of photoefficiency in TiO₂ aqueous suspensions: Effect of titania hydrodynamic particle size and catalyst loading on their optical properties", *Appl. Cat. B: Env.* 221, 1-8
- [46] J. Miao, R. Zhang, L. Zhang, 2018, "Photocatalytic degradations of three dyes with different chemical structures using ball-milled TiO₂", *Materials Research Bulletin* 97, 109-114.
- [47] J. I. Goldstein, D. E. Newbury, P. Echlin, D. C. Joy, C. E. Lyman, E. Lifshin, L. C. Sawyer, J. R. Michael, 2003, "Scanning Electron Microscopy and X-Ray Microanalysis", Springer, ISBN 0306472929.

- [48] G. Varga, J. Kovacs, Z. Szalai, C. Cserhati, G. Ujvari, 2018, “Granulometric characterization of paleosols in loess series by automated static image analysis”, *Sed. Geol.* 370, 1-14.
- [49] K.K Beltrame, A.L. Cazetta, P.S.C. de Souza, L. Spessato, T.L. Silva, V.C. Almeida, 2018, “Adsorption of caffeine on mesoporous activated carbon fibers prepared from pineapple plant leaves”, *Ecotoxicology and Environmental Safety* 147, 64-71.
- [50] S. Zhou, C. Di Paolo, X. Wu, Y. Shao, T-B. Seiler, H. Hollert, 2019, “Optimization of screening-level risk assessment and priority selection of emerging pollutants – The case of pharmaceuticals in European surface waters”, *Environmental International* 128, 1-10.
- [51] I. Langmuir, 1917, “The constitution and fundamental properties of solids and liquids. II. Liquids.”, *J. Am. Chem. Soc.* 39 (9), 1848-1906.
- [52] L. Pan, Y. Matsui, T. Matsushita, N. Shirasaki, 2016, “Superiority of wet-milled over dry-milled superfine powdered activated carbon for adsorptive 2-methylisoborneol removal”, *Wat. Res.* 102, 516-523.
- [53] R.J. Jonge, A.M. Breure, J.G. Van Andel, 1996, “Reversibility of adsorption of aromatic compounds onto powdered activated carbon (PAC)”, *Wat. Res.* 30 (4), 883-892.
- [54] S. Sicar, J.R. Hufton, 2000, “Why does the linear driving force model for adsorption kinetics work?”, *Adsorption* 6, 137-147.
- [55] V. Goetz, J.P. Cambon, D. Sacco, G. Plantard, 2009, “Modeling aqueous heterogeneous photocatalytic degradation of organic pollutants with immobilized TiO₂”, *Chem. Eng. & Process.: Proc. Int.* 48 (1), 532-537.
- [56] A. Joly, A. Perrard, 2009, “Linear driving force models for dynamic adsorption of volatile organic compound traces by porous adsorbent beds”, *Math. & Comp. in Simul.* 79 (12), 3492-3499.
- [57] G. Plantard, T. Janin, V. Goetz, S. Brosillon, 2012, “Solar photocatalysis treatment of phytosanitary refuses: Efficiency of industrial photocatalysts”, *Appl. Cat. B: Env.* 115-116, 38-44.
- [58] J-M. Herrmann, 1999, “Heterogeneous photocatalysis: fundamentals and applications to the removal of various types of aqueous pollutants”, *Cat. Tod.* 53, 115-129.

- [59] K. Vasanth Kumar, K. Prokodi, F. Rocha, 2008, “Langmuir-Hinshelwood kinetics – A theoretical study”, *Cat. Comm.* 9 (1), 82-84.
- [60] M. Mubeen, K. Deshmukh, D.R. Peshwe, S.J. Dhoble, A.D. Deshmukh, 2019, “Alteration of the electronic structure and the optical properties of graphitic carbon nitride by metal ion doping”, *Spectroch. Act. Part. A: Mol. & Biomol. Spec.* 207, 301-306.
- [61] C. Russo, B. Apicella, J.S. Lighty, A. Ciajolo, A. Tregrossi, 2017, “Optical properties of organic carbon and soot produced in an inverse diffusion flame”, *Carbon* 124, 372-379.
- [62] J. Fournier, G. Boiteux, G. Seytre, 1997, “Fractal analysis of percolation network in epoxy – polypyrrole composites”, *Am. Phys. Soc.* 56, 5207– 5212.
- [63] S. Kirkpatrick, 1973, “Percolation and conduction”, *Rev. Mod. Phys.* 45, 574–588.
- [64] L.E. Holman, H. Leuenberger, 1990, “The effect of varying the composition of binary powder mixtures and compacts on their properties: a percolation phenomenon”, *Powder Technol.* 60, 249– 258.
- [65] A. Malliaris, D.T. Turner, 1971, “Influence of particule size on the electrical resistivity of compacted mixtures of polymeric and metallic powders”, *J. Appl. Phys.* 42, 614– 618.
- [66] G. Plantard and M. Papini, 2002, “Radiative and electrical properties of granular materials: Application to mixtures of insulating and conducting polymers”, *Journal of Quantitative Spectroscopy and Radiative Transfer* 74 (3), 329-337.
- [67] O. Carp, C.L. Huisman, A. Reller, 2004, “Photoinduced reactivity of titanium dioxide”, *Progress in Solid State Chemistry* 32, 33-177.
- [68] C. Guillard, J. Disdier, C. Monnet, J. Dussaud, S. Malato, J. Blanco, M.I. Maldonado, J.M. Herrmann, 2003, “Solar efficiency of a new deposited titania photocatalyst: chlorophenol, pesticide and dye removal applications”, *Applied Catalysis B: Environmental* 46, 319-332.
- [69] A.V. Emeline, V. Ryabchuk, N. Serpone, 2000, “Factors affecting the efficiency of a photocatalysed process in aqueous metal-oxide dispersions Prospect of distinguishing between two kinetic models”, *Journal of photochemistry and photobiology* 133, 89-97.
- [70] L. Davydov, P.G. Smirniotis, 2000, “Quantification of the primary processes in aqueous heterogeneous photocatalysis using single-stage oxidation reactions”, *Journal of Catalysis* 191, 105-115.

- [71] J.R. Brandi, A.M. Citroni, O.M. Alfano, A.E. Cassano, 2003, "Absolute quantum yields in photocatalytic slurry reactors", *Chemical Engineering Science* 58, 979 – 985.
- [72] A. Cassano, C. Martin, J.R. Brandi, O.M. Alfano, 1995, "Photoreactor analysis and design: Fundamentals and applications", *Ind. & Ing. Chem. Res.* 34, 2155-2201.
- [73] C.A. Martin, M.A. Baltanas, A. Cassano, 1996, "Photocatalytic reactors II quantum efficiencies allowing for scattering effects. An experimental approximation", *J Photochem. & photobiol A: Chem* 94, 173-189.
- [74] N. Serpone, 1997, "Relative photonic efficiencies and quantum yields in heterogeneous photocatalysis", *J. Photochem & Photobiol A: Chem.* 104, 1-12.
- [75] N. Serpone, S. Angela, 1999, "Terminology, relative photonic efficiencies and quantum yields in heterogeneous photocatalysis. part i: suggested protocol international union of pure and applied chemistry organic chemistry division commission on photochemistry", *Pure & Appl. Chem* 71, 303–320.
- [76] G. Plantard, F. Correia, V. Goetz, 2011, "Kinetic and efficiency of TiO₂-coated on foam or tissue and TiO₂-suspension in a photocatalytic reactor applied to the degradation of the 2,4-Dichlorophenol", *J. Photochem. & photobiol.* 222, 111-116.
- [77] G. Plantard and V. Goetz, 2014, "Correlations between optical, specific surface and photocatalytic properties of media integrated in a photo-reactor", *Chem. of Eng. J.* 252, 194-201.
- [78] K. Elatmani, G. Plantard, D. Sacco, I. Aitichou and V. Goetz, 2013, "Innovative photocatalytic media optimized for solar-powered remediation: application to pyrimethanil", *Mat. Sci. Semicond. Proc.* 16, 1117-1124.
- [79] J. Marugan, D. Hufschmidt, M.J. Lopez-Munoz, V. Selzer, D. Bahnemann, 2006, "Photonic efficiency for methanol photooxydation and hydroxyl radical generation on silica-supported TiO₂ photocatalysts", *Appl. Cat. B* 62, 201-207.

Figure captions

Figure 1. Scanning electron images (SEM-FEG, Hitachi S-4500). Left to right: increasing composite AC percentage as shown on the top. Top to bottom: increasing magnification, as shown on the left.

Figure 2. Granulometric analysis of composites powders for different milling time (i.e. 1h (\square) and 10h (\blacksquare)) and for different AC/TiO₂ composition : 75_ AC/TiO₂ (A) ; 30_AC/TiO₂ (B) ; 15_AC/TiO₂ (C) ; 5_AC/TiO₂ (D) ; 1_AC/TiO₂ (E).

Figure 3. Adsorption isotherms (A) for Caffeine onto RAW Activated Carbon (\blacksquare), M-AC (\bullet). Comparison with Activated Carbon/TiO₂ composites prepared by mechanosynthesis: 1_AC/TiO₂ (-) ; 5_AC/TiO₂ (+) ; 15_AC/TiO₂ (*) ; 30_AC/TiO₂ (\blacktriangle) ; 75_AC/TiO₂ (\blacklozenge).

Figure 4. Caffeine adsorption kinetics of milled AC (\bullet), milled TiO₂ (\circ) and composites powders : 1_CA/TiO₂ (-) ; 5_CA/TiO₂ (+) ; 15_CA/TiO₂ (*) ; 30_CA/TiO₂ (\blacktriangle) ; 75_CA/TiO₂ (\blacklozenge). Dashed lines represent the linear driving force model fitting.

Figure 5. Caffeine removal through time: adsorption and photodegradation (A). Experimental photodegradation kinetics were fitted by a zero-order law reported by lines on graph (B) for all samples : Milled-TiO₂ (\circ) ; 1_AC/TiO₂ (-) ; 5_AC/TiO₂ (+) ; 15_AC/TiO₂ (*) ; 30_AC/TiO₂ (\blacktriangle) ; 75_AC/TiO₂ (\blacklozenge).

Figure 6. Adsorption and photocatalytic related normalized constants reported as a function of AC content within the AC/TiO₂ composite powders: q_{\max} (\blacklozenge) ; b (\circ) ; k_{ads} (\blacktriangle) and α_{app} (\blacksquare).

Figure 7. Number of molecules degraded as a function of (i) the number of incident photons on the suspension (A) ; (ii) the number of incident photons on TiO₂ fraction (B). M-AC (\bullet), M-TiO₂ (\circ) and all composites powders have been reported: 1_AC/TiO₂ (-) ; 5_AC/TiO₂ (+) ; 15_AC/TiO₂ (*) ; 30_AC/TiO₂ (\blacktriangle) and 75_AC/TiO₂ (\blacklozenge).

Table legends

Table 1. EDS analysis: mean values of composition and calculated standard deviation for each composite powder.

Table 2. Granulometric analysis gaussian function fitting parameters for all composite powders.

Table 3. Adsorption and photocatalytic properties related parameters summary for each composite powder.

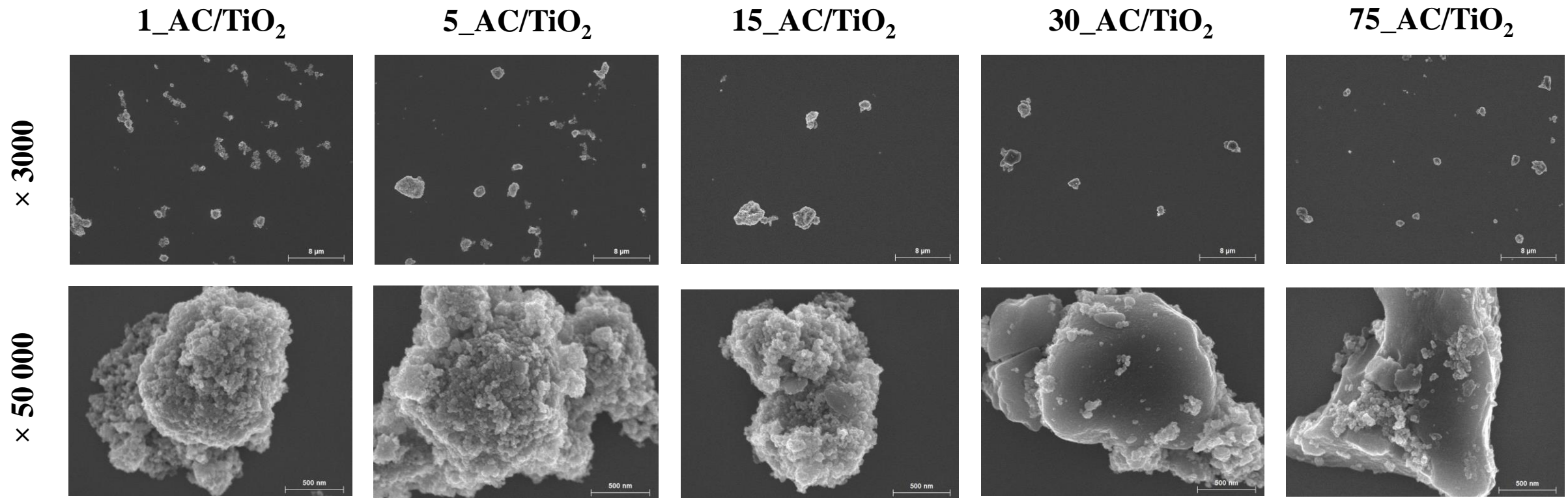


Figure 1. Scanning electron images (SEM-FEG, Hitachi S-4500). Left to right : increasing composite AC percentage as shown on the top. Top to bottom : increasing magnification, as shown on the left.

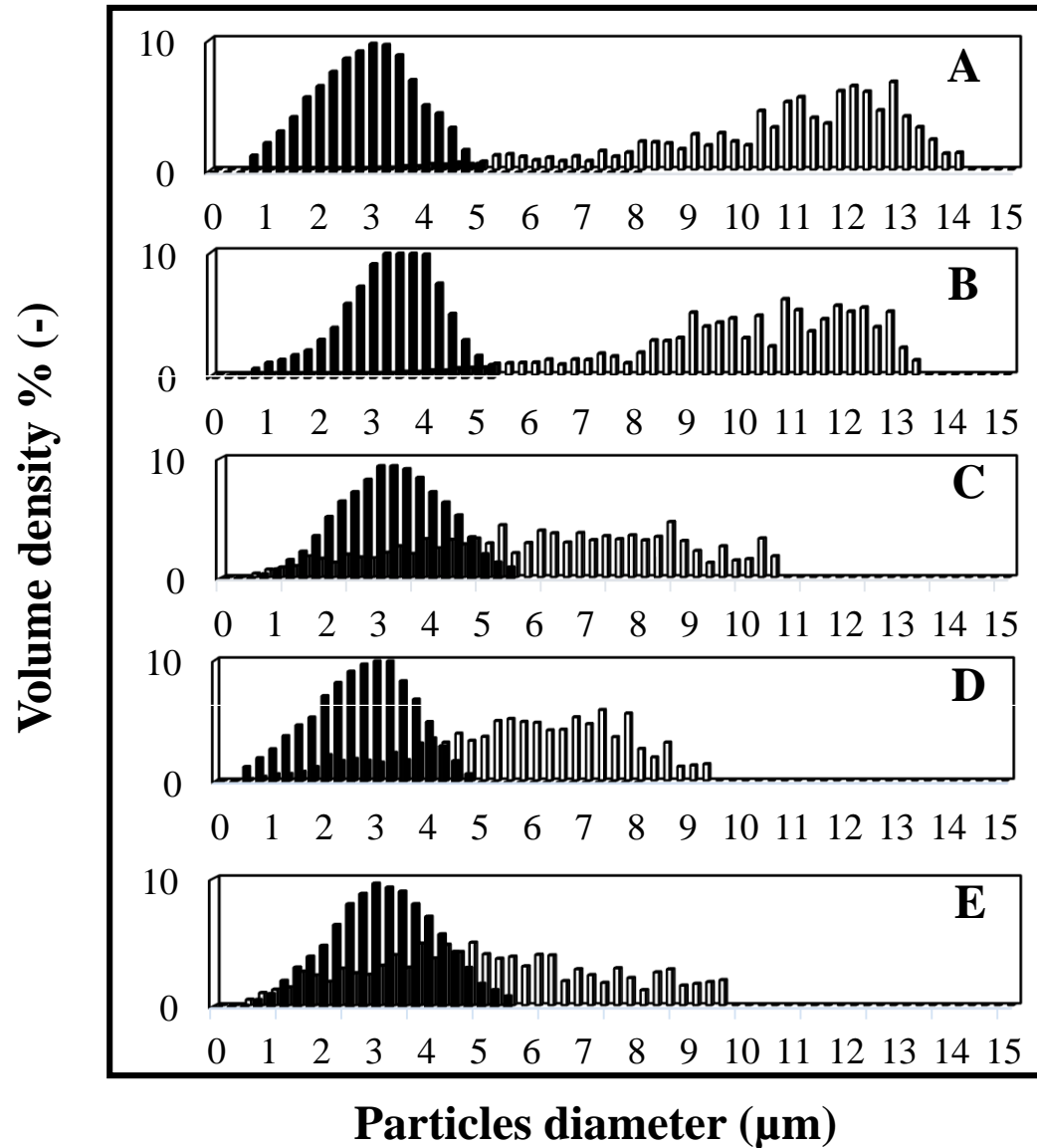


Figure 2. Granulometric analysis of composite powders for different milling time (i.e. 1h (\square) and 10h (\blacksquare)) and for different AC/TiO₂ composition : 75_AC/TiO₂ (A) ; 30_AC/TiO₂ (B) ; 15_AC/TiO₂ (C) ; 5_AC/TiO₂ (D) ; 1_AC/TiO₂ (E).

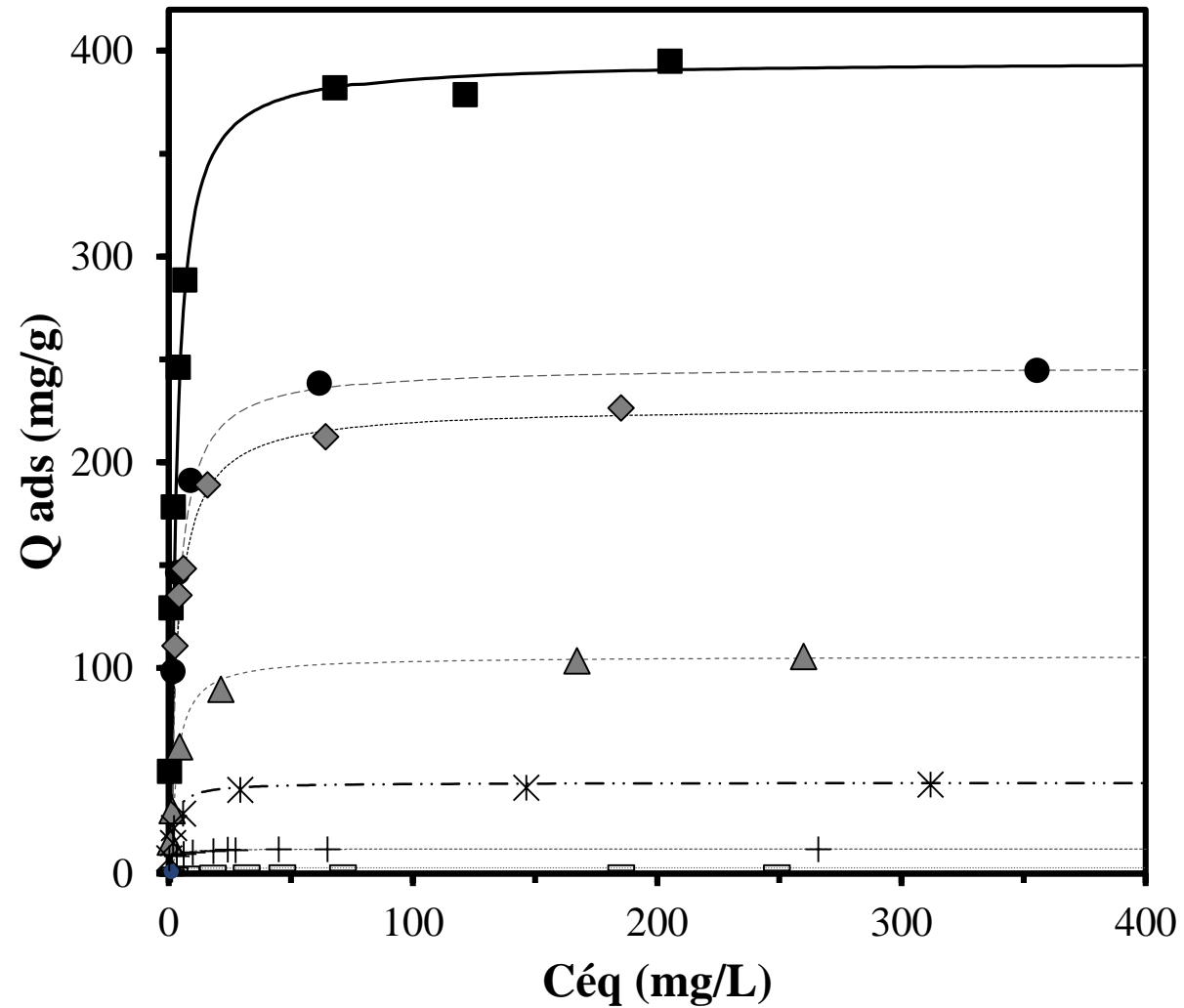


Figure 3. Adsorption isotherms for Caffeine onto RAW Activated Carbon (■), M-AC (●) . Comparison with AC/TiO₂ composites prepared by mechano-synthesis: 1_AC/TiO₂ (■) ; 5_AC/TiO₂ (+) ; 15_AC/TiO₂ (*) ; 30_AC/TiO₂ (▲) ; 75_AC/TiO₂ (◆).

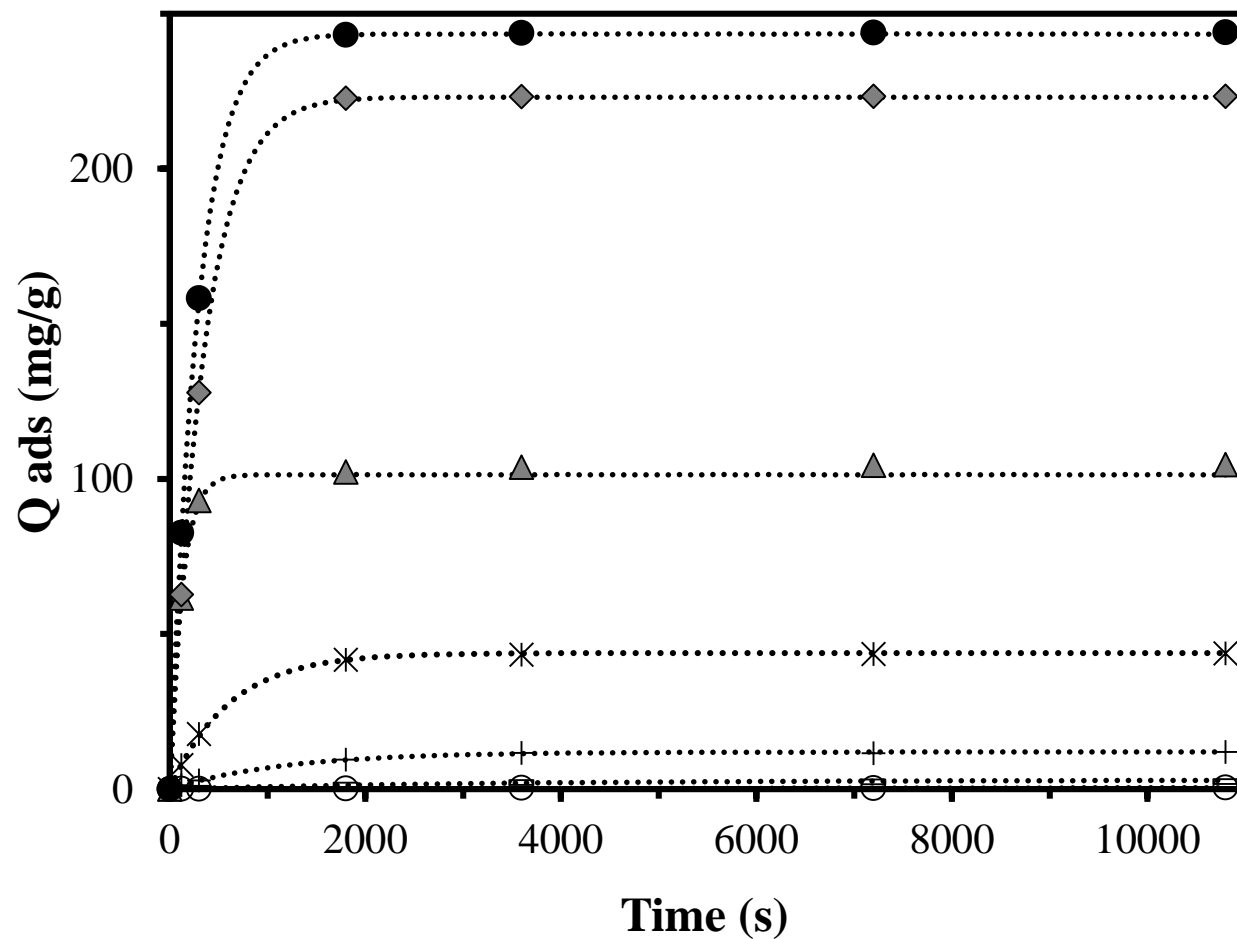


Figure 4. Caffeine adsorption kinetics of milled AC (●), milled TiO_2 (○) and composites powders : 1_CA/ TiO_2 (-); 5_CA/ TiO_2 (+); 15_CA/ TiO_2 (*); 30_CA/ TiO_2 (▲); 75_CA/ TiO_2 (◆). Dashed lines represent the linear driving force model fitting.

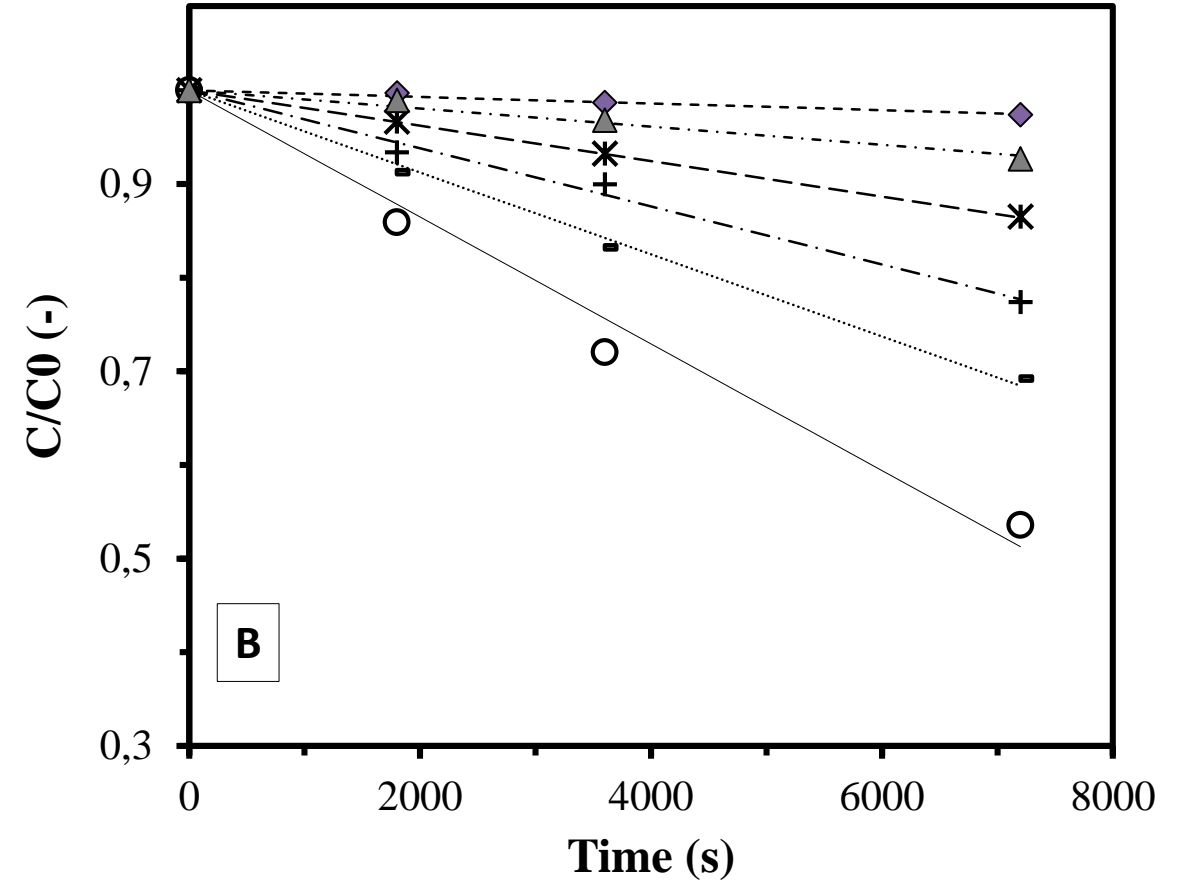
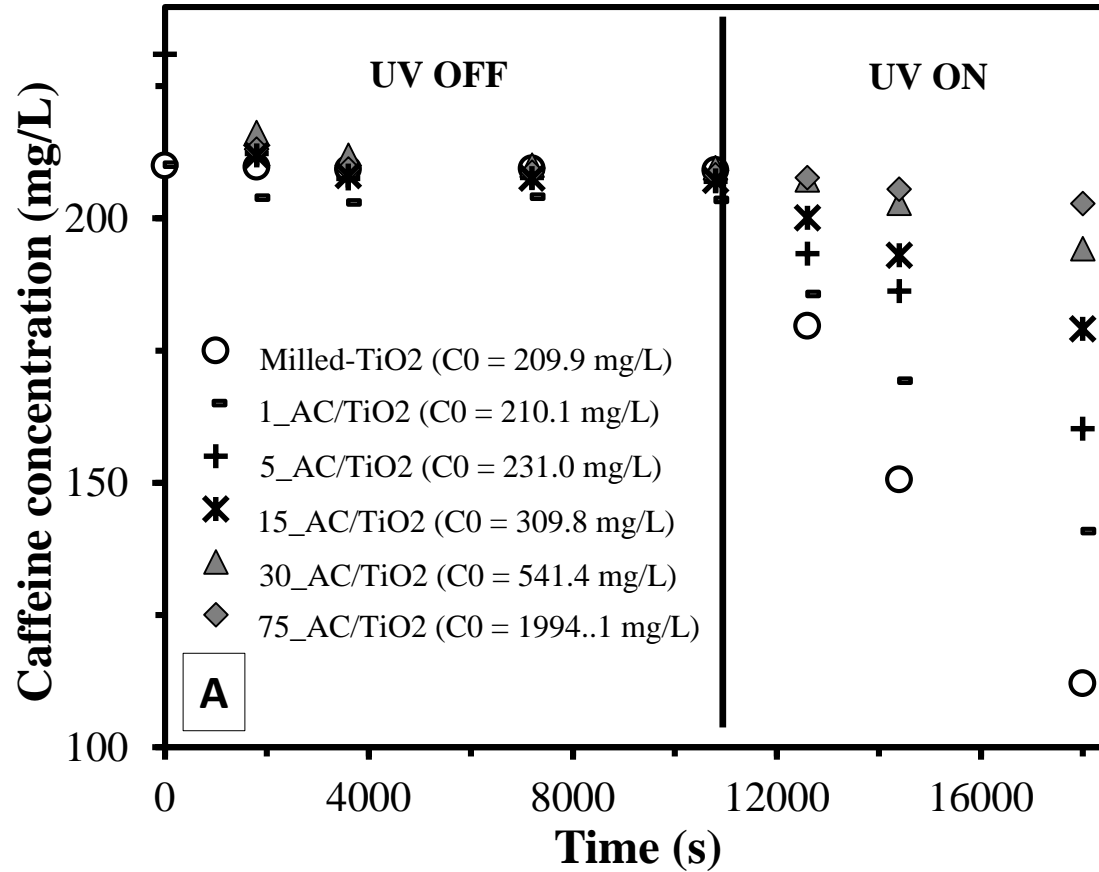


Figure 5. Caffeine removal through time : adsorption and photodegradation (A). Experimental photodegradation kinetics were fitted by a zero-order law reported by lines on graph (B) for all samples : Milled-TiO₂ (○) ; 1_AC/TiO₂ (-) ; 5_AC/TiO₂ (+) ; 15_AC/TiO₂ (*) ; 30_AC/TiO₂ (▲) ; 75_AC/TiO₂ (◆).

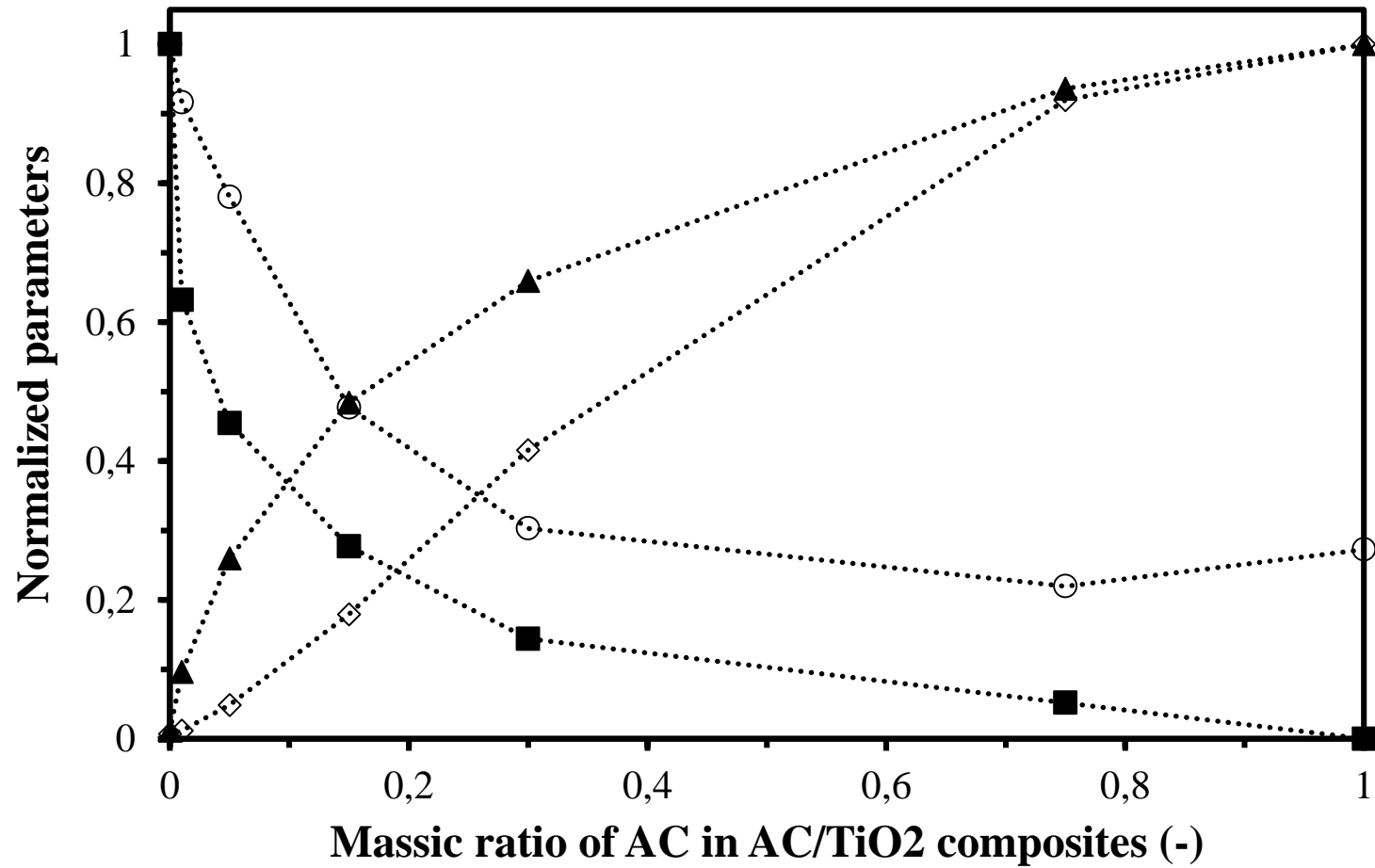


Figure 6. Adsorption and photocatalytic related normalized constants reported as a function of AC content within the AC/TiO₂ composite powders: Q_{max} (◇) ; b (○) ; k_{ads} (▲) and α_{app} (■).

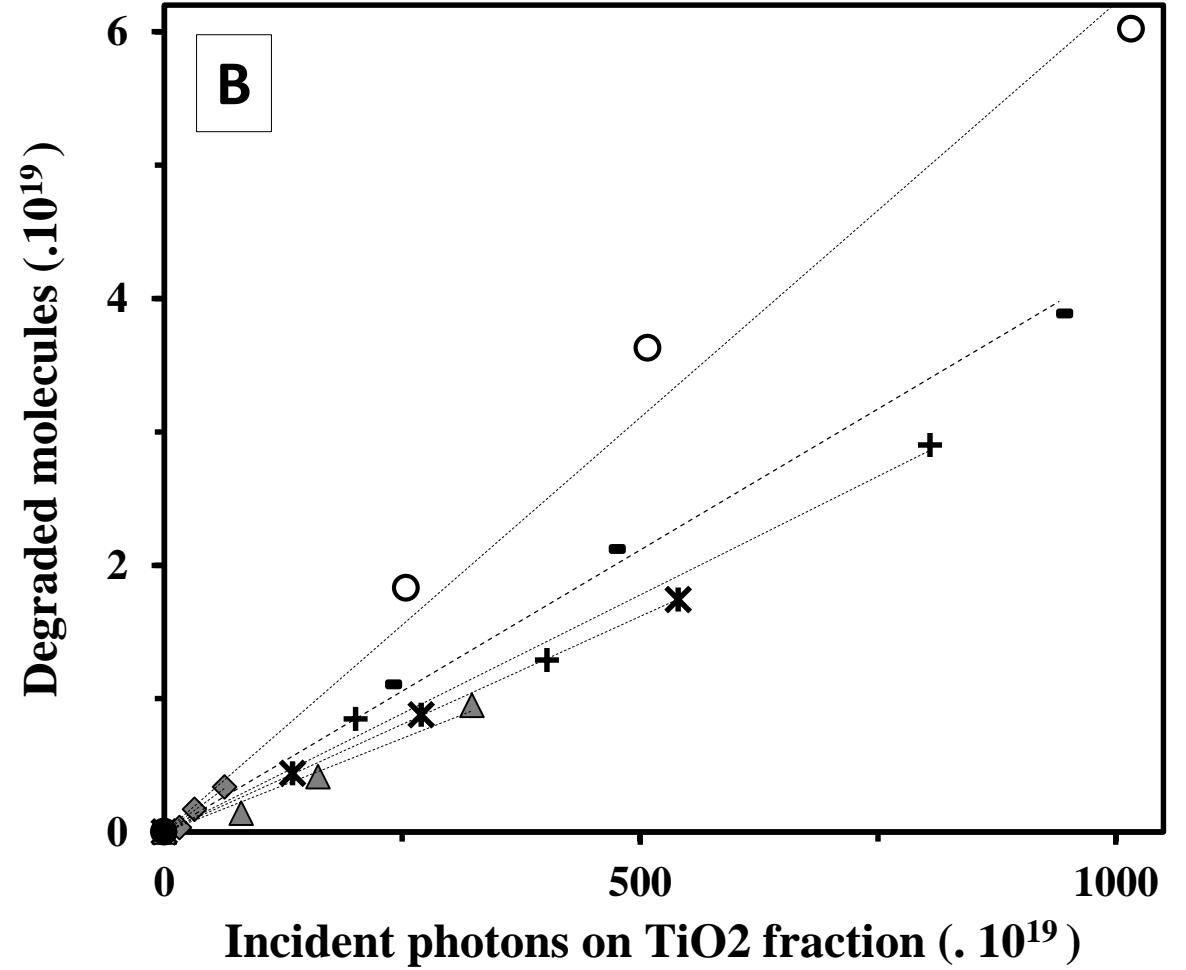
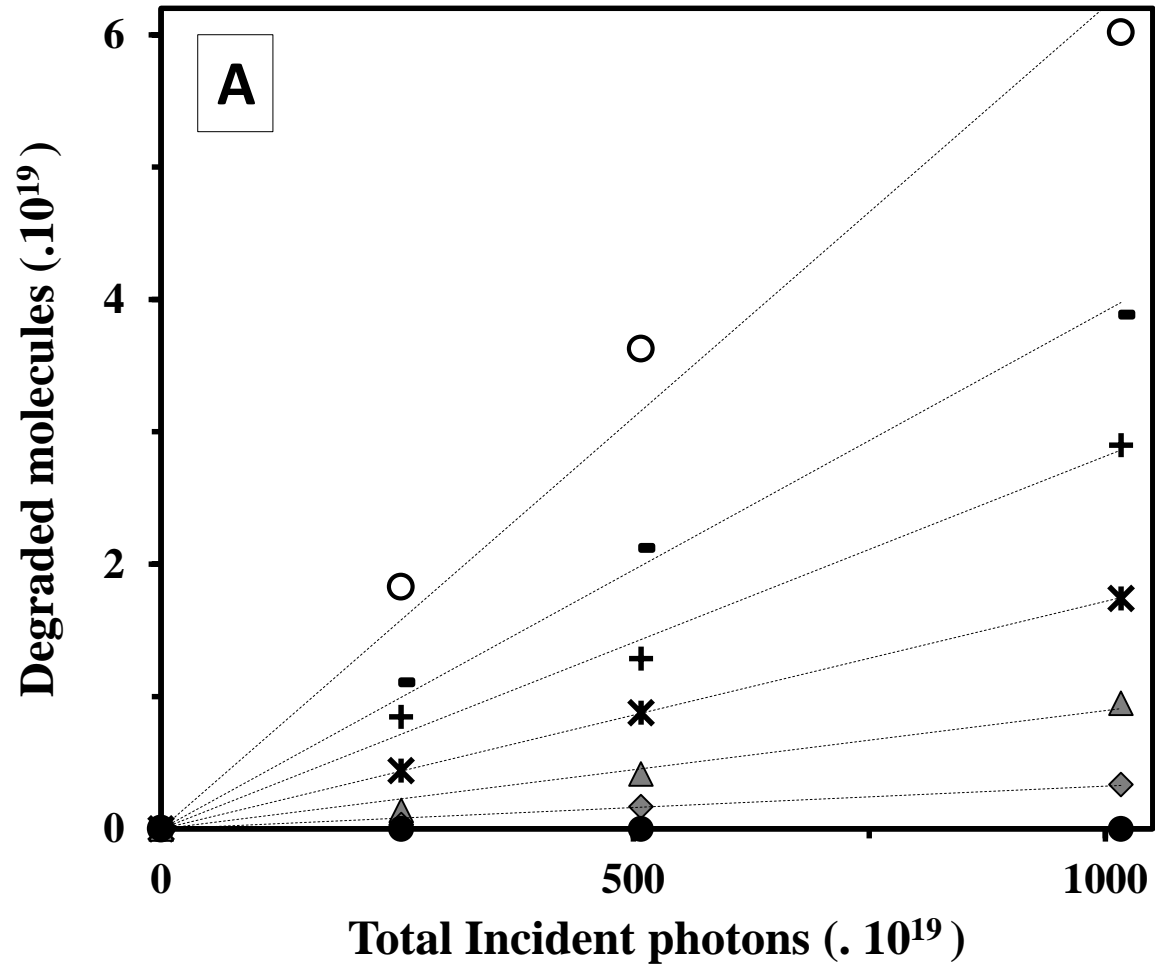


Figure 7. Number of molecules degraded as a function of (i) the number of incident photons on the suspension (A) ; (ii) the number of incident photons on TiO₂ fraction (B). M-AC (●), M-TiO₂ (○) and all composites powders have been reported: 1_AC/TiO₂ (-) ; 5_AC/TiO₂ (+) ; 15_AC/TiO₂ (*) ; 30_AC/TiO₂ (▲) and 75_AC/TiO₂ (◆).

Samples	C		O		Ti	
	wt. %	Std. Deviation %	wt. %	Std. Deviation %	wt. %	Std. Deviation %
1_AC/TiO ₂	3.0	2.0	37.7	5.2	59.3	6.6
5_AC/TiO ₂	6.5	3.2	37.3	4.7	56.2	5.4
15_AC/TiO ₂	14.6	4.5	35.5	5.1	49.9	3.3
30_AC/TiO ₂	29.5	3.9	29.4	4.1	41.1	3.4
75_AC/TiO ₂	76.1	7.5	9.9	3.9	14.0	5.6

Table. 1 EDS analysis : mean values of composition and calculated standard deviation for each composite powder

Gaussian function parameters	Composite samples				
$f(x) = \frac{1}{\sigma\sqrt{2\pi}} e^{-\frac{1}{2}\left(\frac{x-\mu}{\sigma}\right)^2}$	1_AC/TIO2	5_AC/TIO2	15_AC/TIO2	30_AC/TIO2	75_AC/TIO2
Distribution mean μ	3.16	2.79	3.25	3.47	2.90
Standard deviation σ	1.05	1.00	1.06	0.85	1.04
Determination coefficient R^2	0.99	0.97	0.99	0.97	0.99

Table 2. Granulometric analysis gaussian function fitting parameters for all composite powders. █

Parameters	units	M_AC	75_AC/TiO2	30_AC/TiO2	15_AC/TiO2	5_AC/TiO2	1_AC/TiO2	M_TiO2
Q_{\max}	mg/g	246,6	226,8	102,5	44,2	12	2,9	1.7
b	L/mg	0,36	0.29	0.40	0,63	1.03	1.21	1.32
k_{ads}	$\times 10^{-4} \text{ s}^{-1}$	34.29	32.1	22,6	16.6	8,9	3.3	0.4
α_{app}	$\times 10^{-3} \text{ mol.L}^{-1} \cdot \text{s}^{-1}$	0.00	0.73	2.03	3.91	6.41	8.91	14.1

Table 3. Adsorption and photocatalytic properties related parameters summary for each composite powder. █